

## Baseline Cold Matter Effects on $J/\psi$ Production in $AA$ Collisions at RHIC

R. Vogt<sup>1,2</sup>

<sup>1</sup>Nuclear Science Division, Lawrence Berkeley National Laboratory,  
Berkeley, CA 94720, USA

<sup>2</sup>Physics Department, University of California, Davis, CA 95616, USA

*Received 10 July 2005*

**Abstract.** We present baseline calculations of initial-state shadowing and final-state absorption effects on  $J/\psi$  production in nucleus-nucleus collisions at the Relativistic Heavy Ion Collider. We show predictions for Au+Au and Cu+Cu collisions at  $\sqrt{S_{NN}} = 200$  GeV and Cu+Cu collisions at  $\sqrt{S_{NN}} = 62$  GeV as a function of the rapidity,  $y$ , and the number of binary nucleon-nucleon collisions,  $N_{\text{coll}}$ .

*Keywords:*  $J/\psi$ , heavy ion collisions

*PACS:* 24.85.+p, 12.38.Bx, 25.75.-q

The nuclear dependence of  $J/\psi$  production has been studied extensively in fixed target nuclear collisions [ 1] where cold matter effects were attributed solely to nuclear absorption. However, the nuclear parton distributions are modified relative to those of free protons. At  $\sqrt{S} = 17.3$  GeV, the modification, referred to here as shadowing, gives a modest enhancement of  $J/\psi$  production at midrapidity since the  $J/\psi$  is produced in the antishadowing region [ 2]. As  $\sqrt{S}$  increases, the momentum fractions,  $x$ , probed by  $J/\psi$  production at  $y = 0$  decrease, leading to stronger shadowing effects at collider energies. New measurements at the Relativistic Heavy Ion Collider (RHIC) on nuclear collisions may determine the importance of dense matter effects on  $J/\psi$  production. For these analyses to be meaningful, it is essential to have a proper baseline for quarkonium suppression in  $AA$  collisions due to cold matter effects.

This paper studies the interplay of shadowing and absorption in nuclear collisions at RHIC. We address both spatially homogeneous (minimum bias) results as a function of rapidity and inhomogeneous (fixed impact parameter) analyses as a function of the number of nucleon-nucleon collisions. Our calculations, described in detail in Ref. [ 3] for d+Au collisions, agree relatively well with the preliminary PHENIX d+Au data [ 4]. Thus if  $J/\psi$  production is unaffected by quark-gluon

plasma formation, these predictions should describe the rapidity and centrality dependence of  $J/\psi$  production in  $AA$  collisions. Since RHIC has completed both Au+Au and Cu+Cu runs at  $\sqrt{S_{NN}} = 200$  GeV and a  $\sqrt{S_{NN}} = 62$  GeV Cu+Cu run, we present predictions for shadowing and absorption effects on  $J/\psi$  production in these three systems.

Our  $J/\psi$  calculations generally employ the color evaporation model (CEM) [5]. The  $J/\psi$  rapidity distribution in an  $AB$  collision at impact parameter  $b$  is

$$\frac{d\sigma}{dyd^2bdzd^2rdz'} = 2F_{J/\psi} \sum_{i,j} \int_{2m_c}^{2m_D} M dM F_i^A(x_1, Q^2, \vec{r}, z) F_j^B(x_2, Q^2, \vec{b} - \vec{r}, z') \frac{\sigma_{ij}}{M^2} \times S_A^{\text{abs}}(\vec{r}, z) S_B^{\text{abs}}(\vec{b} - \vec{r}, z'). \quad (1)$$

where  $x_{1,2} = (M/\sqrt{S_{NN}}) \exp(\pm y)$  at leading order. The parameter  $F_{J/\psi}$  is the fraction of  $c\bar{c}$  pairs below the  $D\bar{D}$  threshold that become  $J/\psi$ 's [5]. Since the shadowing ratios are independent of the order of the calculation [6, 7], the  $AA/pp$  ratios are calculated at leading order to speed the numerics. We use  $m_c = 1.2$  GeV and  $Q = M$  [5] with the MRST LO parton densities [8].

The parton densities in the nucleus,  $F_i^A(x, Q^2, \vec{r}, z) = \rho_A(s) S_{P,S}^i(A, x, Q^2, \vec{r}, z) f_i^N(x, Q^2)$ , are the product of the nucleon density [9],  $\rho_A(s)$ , the nucleon parton density,  $f_i^N(x, Q^2)$ , and a shadowing ratio,  $S_{P,S}^i(A, x, Q^2, \vec{r}, z)$ , where  $\vec{r}$  and  $z$  are the transverse and longitudinal position of the parton with  $s = \sqrt{r^2 + z^2}$ . The two subscripts on  $S_{P,S}^i$  refer to the shadowing parameterization and the spatial dependence, respectively. Most of our results are presented for the EKS98 shadowing parameterization [10] but we also compare to predictions with the three FGS parameterizations [11]: FGS<sub>o</sub>, FGS<sub>h</sub> and FGS<sub>l</sub>. Since  $A = 63$  is not available from FGS, the results here are calculated with  $A = 40$ .

Figure 1(a) compares the four homogeneous gluon ratios,  $S_{\text{EKS}}^g$  and  $S_{\text{FGSi}}^g$  for  $Q = 2m_c$ . The thin curves are for  $A = 197$  while the thick curves show  $A = 63$  ( $A = 40$  for FGS). FGS predicts more shadowing at small  $x$ . The decrease of shadowing with  $A$  is stronger for FGS since a smaller  $A$  is used. The EKS98 and FGS<sub>l</sub> ratios for the lighter  $A$  are very similar for  $0.001 < x < 0.2$ . While all parameterizations show significant antishadowing, the EKS98 antishadowing  $x$  range is larger. Shadowing alone will give an effective  $A$  dependence as a function of rapidity with  $y > 0$  corresponding to low  $x_2$ , effectively mirroring the curves in Fig. 1(a) for  $dA$  while, in  $AA$  collisions, the result should be similar to the product of the curves with their mirror images.

Figure 1(b) shows the average value of  $x_2$  for  $\sqrt{S_{NN}} = 200$  (solid) and 62 (dashed) GeV. At midrapidity at 200 GeV,  $\langle x_2 \rangle \sim 0.01$ , near the point where  $S_P^g \leq 1$ . In the forward region,  $\langle x_2 \rangle \sim 10^{-3}$  at  $y \sim 2$ , clearly in the effective low  $x$  regime while for negative rapidity,  $y \sim -2$ ,  $\langle x_2 \rangle \sim 0.1$ , in the antishadowing region. At 62 GeV, the average  $\langle x_2 \rangle$  is larger and the rapidity distribution is narrower. At midrapidity,  $\langle x_2 \rangle \sim 0.05$ , in the antishadowing region. Thus, the predicted shadowing effects should be quite different for the two energies, as we will show.

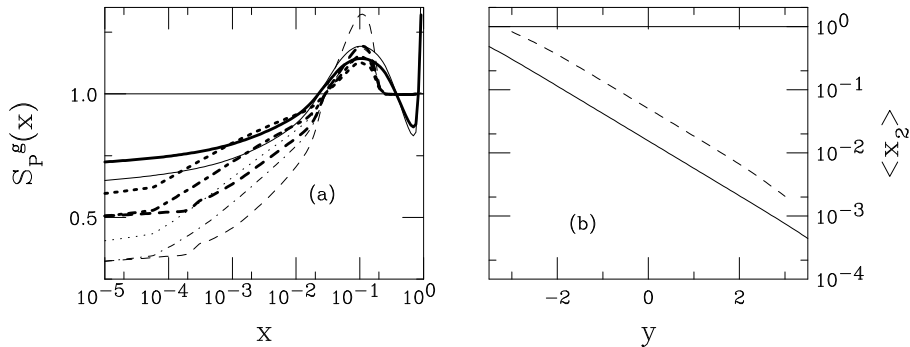


**Fig. 1.** (a) The gluon shadowing parameterizations at scale  $\mu = 2m = 2.4$  GeV for EKS98 (solid), FGSo (dashed), FGSh (dot-dashed) and FGS1 (dotted). The thin curves are for Au while the thick curves are for Cu (Ca for the FGS parameterizations). (b) The average value of  $x_2$  in  $pp$  collisions as a function of  $y$  for  $\sqrt{S} = 200$  (solid) and 62 (dashed) GeV.

We assume that the inhomogeneous EKS98 and FGSo parameterizations are proportional to the parton path through the nucleus,  $S_{P,\rho}^i$  [6], normalized so that  $(1/A) \int d^2r dz \rho_A(s) S_{P,\rho}^i(A, x, Q^2, \vec{r}, z) = S_P^i(A, x, Q^2)$ . The inhomogeneous FGS parameterizations are normalized so that  $(1/A) \int d^2s T_A(s) S_{FGSh,l}^i(A, x, Q^2, \vec{s}) = S_{FGSh,l}^i(A, x, Q^2)$ .

The survival probability,  $S_A^{\text{abs}}$ , for  $J/\psi$  absorption by nucleons is  $S_A^{\text{abs}}(\vec{r}, z) = \exp\left\{-\int_z^\infty dz' \rho_A(\vec{r}, z') \sigma_{\text{abs}}(z' - z)\right\}$  where  $z$  is the production point and  $z'$  is the absorption point. We consider both color octet and singlet absorption. The octet  $|(c\bar{c})_{8g}\rangle$  state can convert to a singlet with a formation time of 0.25 fm at negative rapidity. Otherwise if the  $J/\psi$ ,  $\psi'$  and  $\chi_c$  hadronize outside the nucleus, they have identical, finite octet cross sections. The singlet cross section grows quadratically with proper time until the formation time of each charmonium state. Thus the individual charmonium states have different asymptotic cross sections depending on their relative radii but absorption is ineffective if the state forms outside the target. See Ref. [12] for more details.

In Fig. 2 we contrast the  $AA/pp$  ratios in Au+Au and Cu+Cu collisions calculated with EKS98 and asymptotic absorption cross sections,  $\sigma_{\text{abs}} = 0, 1, 3$  and 5 mb, for octet absorption (upper plots) and color singlet absorption (lower plots). The zero value illustrates the effects of shadowing alone. A 3 mb absorption cross section was needed to obtain agreement with the E866 800 GeV  $J/\psi$  data [13] at  $x_F \approx 0$  [14]. The absorption cross section has been predicted to both decrease [15] and increase [16] with energy. The PHENIX d+Au data [4] suggest  $\sigma_{\text{abs}} \leq 3$  mb at RHIC [3], in accord with a constant or decreasing  $\sigma_{\text{abs}}$ .

The  $AA/pp$  ratios are symmetric around  $y = 0$ . The effect of octet to singlet conversion at large  $y$  is negligible for  $\sqrt{S_{NN}} = 200$  GeV when  $\sigma_{\text{abs}} > 2.5$  mb, the

singlet cross section assumed in the model [ 17]. The results with singlet absorption differ from those with shadowing alone only at  $|y| \geq 1-2$  at 200 GeV and  $|y| \geq 0.5-1$  at 62 GeV. The larger values of  $\sigma_{\text{abs}}$  correspond to the greater rapidity range. Formation is within the 'target' at negative rapidity and within the 'projectile' at positive rapidity.

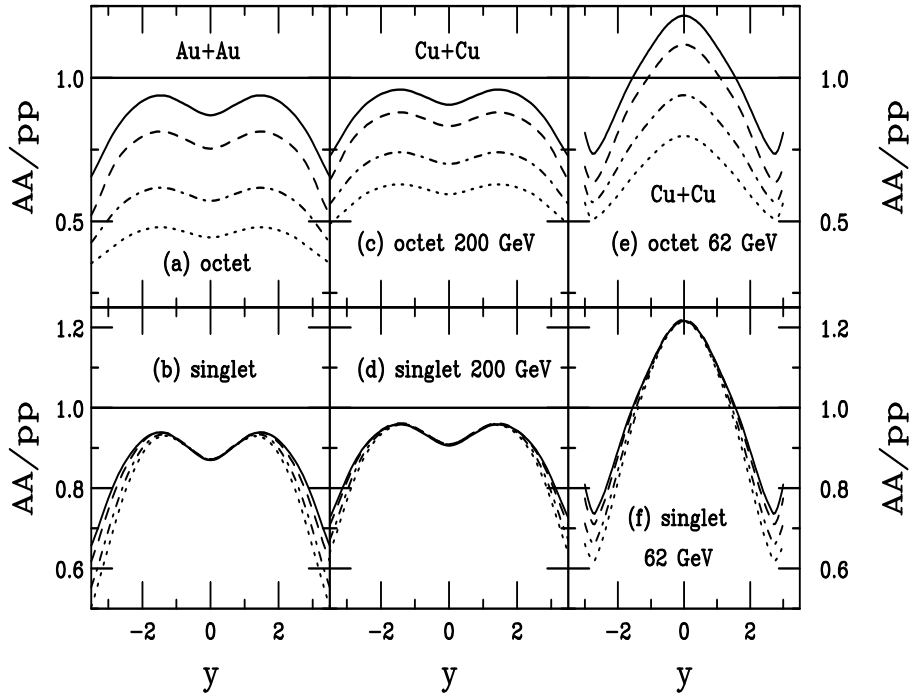


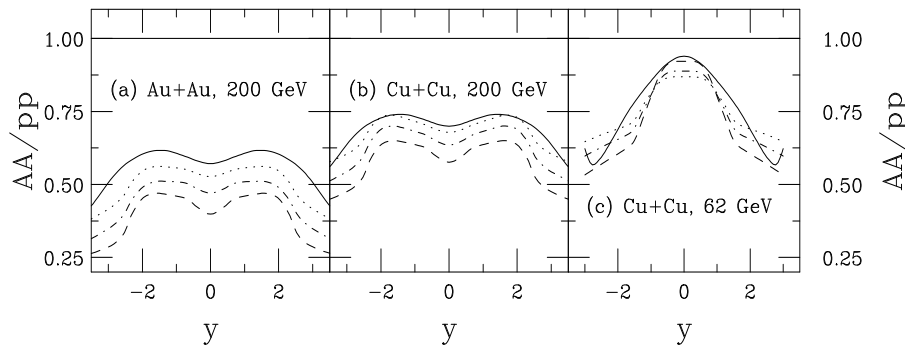
**Fig. 2.** The  $AA/pp$  ratio with the EKS98 parameterization as a function of  $y$  for octet (upper) and singlet (lower) absorption. In (a) and (b) we show the Au+Au results at 200 GeV while the Cu+Cu results are shown at 200 GeV (c) and (d) as well as at 62 GeV (e) and (f). The curves are  $\sigma_{\text{abs}} = 0$  (solid), 1 (dashed), 3 (dot-dashed) and 5 mb (dotted).

There are two peaks in the 200 GeV ratios at  $y \approx \pm 1.5$ , the location of the antishadowing peak at  $x \approx 0.1$ . There is a dip at  $y = 0$  where the shadowing region in  $x$  of one nucleus coincides with the EMC  $x$  region of the other. The convolution of the two shadowing ratios causes  $AA/pp < 1$  over all  $y$  rather than a ratio greater than unity in some regions, as in  $dAu/pp$  [ 3]. The results are similar for Au+Au and Cu+Cu except for the relative magnitude since shadowing and absorption effects are both reduced for the smaller  $A$ .

On the other hand, at  $\sqrt{S_{NN}} = 62$  GeV, the antishadowing regions of the two nuclei coincide, giving a peak with  $AA/pp > 1$  for  $y \approx 0$ . Away from midrapidity,

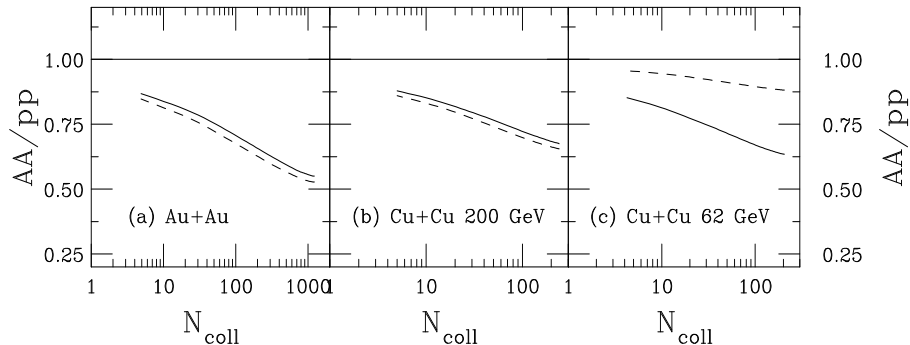
the ratio decreases until  $y \approx \pm 2.5$  where  $x$  is in the ‘Fermi motion’ regime, approaching the edge of phase space. Note also that at the lower energy the  $J/\psi$  can be absorbed inside the target over a larger range of  $y$  since the effective formation time is shorter at the lower energy.

Figure 3 compares the shadowing parameterizations for the three systems assuming octet absorption with  $\sigma_{\text{abs}} = 3$  mb. The differences are largest for Au+Au, the only system where the EKS98 and FGS parameterizations can directly be compared since  $A = 197$  is an option for them all (except FGS0 which takes  $A = 206$ ). The differences between the shadowing parameterizations are larger in  $AA$  than in  $dA$  collisions since the combination of two nuclei enhances the differences. Since the parameterizations are most similar in the antishadowing region, the range of predictions is reduced at  $\sqrt{S_{NN}} = 62$  GeV.



**Fig. 3.** The ratio  $AA/pp$  as a function of  $y$  for octet absorption with  $\sigma_{\text{abs}} = 3$  mb and the EKS98 (solid), FGS0 (dashed), FGSsh (dot-dashed) and FGS1 (dotted) parameterizations for Au+Au at 200 GeV (a) and Cu+Cu at 200 GeV (b) and 62 GeV (c).

Finally, the spatial dependence of the  $AA/pp$  ratios are shown in Fig. 4 for the three systems as a function of the number of binary nucleon-nucleon collisions,  $N_{\text{coll}}$ , assuming  $\sigma_{\text{abs}} = 3$  mb. We have chosen two rapidities to illustrate the results:  $y = 0$  (dashed) and 2 (solid), corresponding to the central and forward regions covered by PHENIX lepton measurements. We do not show the equivalent backward region,  $y = -2$ , since they are identical to those at  $y = 2$ . The EKS98 results shown here are very similar to the FGS predictions, even those with inhomogeneous parameterizations. Note that if a smaller  $\sigma_{\text{abs}}$  is required by the rapidity-dependent data, the ratios shown here would be closer to unity. One might naively expect that the ratios at  $y = 2$  would be lower than those at  $y = 0$  since  $x_2$  is lower than at midrapidity but because  $y = 2$  is in the antishadowing region of  $x_1$  at 200 GeV, its ratio is higher. On the other hand, at 62 GeV and  $y = 2$ ,  $x_2$  is in the shadowing regime while  $x_1$  is in the EMC regime, making the ratio lower. In the backward region,  $x_2$  and  $x_1$  are interchanged but the results remain identical.



**Fig. 4.** The ratio  $AA/pp$  as a function of  $N_{\text{coll}}$  for a 3 mb octet absorption cross section and the EKS98 parameterization at  $y = 0$  (dashed) and  $y = 2$  (solid) for Au+Au at 200 GeV (a) and Cu+Cu at 200 GeV (b) and 62 GeV (c).

The results are shown as a function of  $N_{\text{coll}}$  since  $J/\psi$  production is presumed to be a hard process. We have not shown the ratios for  $b > 2.1R_A$  where  $N_{\text{coll}} \rightarrow 1$ . The number of nucleon-nucleon collisions in Au+Au is considerably larger than the maximum  $N_{\text{coll}}$  for Cu+Cu. Since the inelastic nucleon-nucleon cross section is lower at 62 GeV,  $N_{\text{coll}}$  is somewhat reduced relative to 200 GeV. The results are similar as a function of the number of participating nucleons,  $N_{\text{part}}$ , the centrality variable for soft particle production. We prefer to discuss  $J/\psi$  production as a function of  $N_{\text{coll}}$  or  $N_{\text{part}}$  since these variables depend only on the nuclear density distributions. No additional model assumptions about the nature of the medium are needed, as is the case for other variables such as the path length,  $L$ , [ 18] or the energy density,  $\epsilon$  [ 19].

PHENIX has shown that these cold matter effects are important in d+Au collisions [ 4]. If there are no additional effects on  $J/\psi$  production in AA collisions, the predictions shown here should describe the AA results. If quark-gluon plasma production causes further  $J/\psi$  suppression in AA interactions, then there should be deviations from this pattern. The extent of these deviations would depend on the rapidity range of the produced plasma. Since dense matter effects seem important for other AA observables [ 20], some additional  $J/\psi$  suppression might be expected. However, recent calculations of lattice-based potential models [ 21] and  $J/\psi$  spectral functions [ 22] show that the  $J/\psi$  itself might not break up until  $T \sim 2.5T_c$ . On the other hand, the  $\psi'$  and  $\chi_c$  contributions, 40% of the yield, should be removed if these states break up at  $0.7 < T/T_c < 1.1$ , as expected. The loss of these contributions should be observable in the rapidity dependent ratios as additional absorption, especially at midrapidity, relative to the dAu/ $pp$  ratios shown in Ref. [ 3].

## Acknowledgments

We thank Mike Leitch for suggesting this work and Olivier Drapier for discussions. This work was supported in part by the Director, Office of Energy Research, Division of Nuclear Physics of the Office of High Energy and Nuclear Physics of the U. S. Department of Energy under Contract Number DE-AC02-05CH11231.

## References

1. B. Alessandro *et al.* (NA50 Collaboration), *Eur. Phys. J.* **C33** (2004) 31.
2. V. Emel'yanov, A. Khodinov, S.R. Klein and R. Vogt, *Phys. Rev.* **C59** (1999) 1860.
3. R. Vogt, *Phys. Rev.* **C71** (2005) 054902.
4. R. de Cassagnac (PHENIX Collaboration), *J. Phys. G* **30** (2004) S1341.
5. R.V. Gavai, D. Kharzeev, H. Satz, G. Schuler, K. Sridhar and R. Vogt, *Int. J. Mod. Phys.* **A10** (1995) 3043; G.A. Schuler and R. Vogt, *Phys. Lett.* **B387** (1996) 181.
6. S.R. Klein and R. Vogt, *Phys. Rev. Lett.* **91** (2003) 142301.
7. R. Vogt, *J. Phys. G* **37** (2005) S773.
8. A.D. Martin, R.G. Roberts, and W.J. Stirling, and R.S. Thorne, *Phys. Lett.* **B443** (1998) 301.
9. C.W. deJager, H. deVries, and C. deVries, *Atomic Data and Nuclear Data Tables* **14** (1974) 485.
10. K.J. Eskola, V.J. Kolhinen and P.V. Ruuskanen, *Nucl. Phys.* **B535** (1998) 351; K.J. Eskola, V.J. Kolhinen and C.A. Salgado, *Eur. Phys. J.* **C9** (1999) 61.
11. L. Frankfurt, V. Guzey and M. Strikman, *Phys. Rev.* **D71** (2005) 054001.
12. R. Vogt, *Nucl. Phys.* **A700** (2002) 539.
13. M.J. Leitch *et al.* (E866 Collaboration), *Phys. Rev. Lett.* **84** (2000) 3256.
14. R. Vogt, *Phys. Rev.* **C61** (2000) 035203.
15. C. Lourenco *et al.* in N. Brambilla *et al.*, arXiv:hep-ph/0412158.
16. D. Kharzeev, M. Nardi and H. Satz in M. Bedjidian *et al.*, arXiv:hep-ph/0311048.
17. D. Kharzeev and H. Satz, *Phys. Lett.* **B366** (1996) 316.
18. C. Gerschel and J. Hüfner, *Z. Phys.* **C56** (1992) 71.
19. J.D. Bjorken *Phys. Rev.* **D27** (1983) 140.
20. I. Arsene *et al.* (BRAHMS Collaboration), *Nucl. Phys.* **A757** (2005) 1; B.B. Back *et al.* (PHOBOS Collaboration), *Nucl. Phys.* **A757** (2005) 28; J. Adams *et al.* (STAR Collaboration), *Nucl. Phys.* **A757** (2005) 102; K. Adcox *et al.* (PHENIX Collaboration), *Nucl. Phys.* **A757** (2005) 184.
21. S. Digal, P. Petreczky and H. Satz, *Phys. Lett.* **B514** (2001) 57; C.-Y. Wong, arXiv:hep-ph/0408020.
22. See *e.g.* M. Asakawa and T. Hatsuda, *Phys. Rev. Lett.* **92** (2004) 012001; S. Datta *et al.*, *Phys. Rev.* **D69** (2004) 094507.